Comparison between optical-model potentials in *G*-matrix folding method and improved local-density approximation method

M. Kohno
Research Center for Nuclear Physics, Osaka University, Ibaraki 567-0047, Japan

(Received 15 November 2019; revised 11 July 2020; accepted 23 July 2020; published 10 August 2020)

Microscopic optical-model potentials evaluated by two methods in a nuclear matter approach, namely a *G*-matrix folding method and an improved local-density approximation (LDA) method, are compared. The real parts agree well and show good correspondence to a phenomenological Woods-Saxon potential when second-order contributions are taken into account. On the other hand, the resemblance is not so good in an imaginary part. The reason for the similarity in the real part of the two methods is examined. The improved LDA, which requires less numerical effort, is useful to apply in other cases such as hyperon potentials.

DOI: 10.1103/PhysRevC.102.024611

I. INTRODUCTION

Nuclear matter is a valuable place to consider nucleon-nucleon correlations in the nuclear medium and to study nuclear bulk properties based on bare nucleon-nucleon interactions. To relate the properties obtained in nuclear matter to those in finite nuclei, a local-density approximation (LDA) has been employed at various stages. The idea of the LDA [1] is based on the assumption that the interaction range is smaller than or comparable to the length scale of the density change in finite nuclei.

In microscopic studies of an optical-model potential (OMP) that describe nucleon-nucleus elastic scattering, a nuclear matter approach [2–6] has been a successful method. The conventional way of applying the *G* matrices in the Brueckner theory evaluated in nuclear matter to describe elastic nucleon-nucleus scattering cross sections is first to parametrize the *G* matrices in a convenient function form as an energy- and density-dependent two-body effective interaction and then to apply it to construct an OMP by a folding procedure with target wave functions. The density-dependence of the effective interaction is treated by a local-density approximation. This method is referred to as a *G*-matrix folding method. The successful calculations in this method by several groups [7–9] indicate that physically important medium effects are properly taken into account together with the regularization of high-momentum singular components of the bare nucleon-nucleon force.

A simpler method of using the *G* matrices in nuclear matter to infer the OMP in finite nuclei is an improved LDA, which was introduced in the early stage of the nuclear matter approach [4] and was shown to work well. In this method, the single-particle potential in nuclear matter calculated by the *G* matrices is directly assigned to the potential at the corresponding density in a nucleus. To simulate finite-range effects, a form factor typically in a Gaussian form with an adequate range is convoluted. Recent investigations [10,11] in the literature sometimes use the LDA and/or improved LDA. If the improved LDA is confirmed to be reliable, the method is useful to be applied in a broader situation such as hyperon-nucleus interactions, because an elaborate fitting of *G* matrices in some function form can be avoided.

The practical success of the improved LDA does not imply that its properties are well understood. The concern noted in the pioneering paper [4] has not been well answered that the introduction of a Gaussian form factor in the improved LDA is only qualitative and the theoretical foundation of the folding formula in the imaginary part is shakier than that of the real part. Therefore, theoretical studies of the improved LDA are meaningful. In this paper, the improved LDA is examined in two ways, numerically and analytically.

First, the OMP obtained by the improved LDA is compared with that of the more elaborate *G*-matrix folding method, employing the same *G* matrices in nuclear matter. If these two potentials are similar, the improved LDA approximation is reassuring to be used as a useful method in discussing microscopic single-particle potentials in the nuclear medium. Next, analytical derivation of the expression of the improved LDA is discussed, starting with the *G* matrices in nuclear matter. It is shown that the Gaussian folded form is obtained by supposing a plausible approximation for *G*-matrix elements.

In Sec. II, after a recapitulation of the two methods, OMPs are numerically evaluated for ^{40}Ca, ^{90}Zr, and ^{208}Pb in the *G*-matrix folding method and the improved LDA method and resulting potentials are compared. The correspondence of these OMPs to a standard phenomenological Woods-Saxon potential is also demonstrated. Theoretical considerations for the reliable reproduction of the real part of the *G*-matrix folding potential by the improved LDA method are given in Sec. III, which indicates what approximation is required to obtain improved LDA expression. The summary follows in Sec. IV.

II. MICROSCOPIC OPTICAL-MODEL POTENTIALS

The basic expressions of the G-matrix folding method and the improved LDA method are recapitulated. A naive folding procedure for effective two-body interactions in a finite nucleus by target single-particle wave functions generates a nonlocal potential. Although there is no problem to solve scattering problems with a nonlocal potential, a localization approximation has been commonly introduced. The standard method was provided by Brieva and Rock [6]. The reliability of the Brieva-Rock localization was demonstrated in Ref. [12]. The localized potential for the nucleon with the incident energy E reads

$$U_\tau(\boldsymbol{r},E)=\sum_{\tau'=p,n}\left\{\int d\boldsymbol{r}'\rho_\tau(\boldsymbol{r}')g^D_{\tau\tau'}(\boldsymbol{s};\rho,E)-\rho_\tau(\boldsymbol{r},\boldsymbol{r}')g^E_{\tau\tau'}(\boldsymbol{s};\rho,E)\right\}, \tag{1}$$

where $\boldsymbol{s}=\boldsymbol{r}-\boldsymbol{r}'$ and ρ represents the density dependence. The effective interaction terms $g^D_{\tau\tau'}$ and $g^E_{\tau\tau'}$ are defined by a combination of the $G^{S,T}$ matrices in the total spin S and the total isospin T state of the two-nucleon pair,

$$g^D_{\tau\tau'}=\sum_{S=0,1;T=0,1}(1/2\tau\,1/2\tau'|T\,\tau+\tau')^2\hat{S}G^{S,T}, \tag{2}$$

$$g^E_{\tau\tau'}=\sum_{S=0,1;T=0,1}(-1)^{S+T}(1/2\tau\,1/2\tau'|T\,\tau+\tau')^2\hat{S}G^{S,T}, \tag{3}$$

where $\hat{S}\equiv 2S+1$. For the exchange density matrix $\rho_\tau(\boldsymbol{r},\boldsymbol{r}')$, the Slater approximation [13,14] is employed:

$$\rho_\tau(\boldsymbol{r},\boldsymbol{r}')\simeq\rho_\tau(\boldsymbol{r}_m)\frac{3}{sk_{F,\tau}(r)}j_1(sk_{F,\tau}), \tag{4}$$

where $\boldsymbol{r}_m=(\boldsymbol{r}+\boldsymbol{r}')/2$ and j_1 is a spherical Bessel function of the first kind. The local Fermi momentum $k_{F,\tau}(r)$ is related to the local density $\rho_\tau(r)$ by $\rho_\tau(r)=\frac{1}{3\pi^2}k^3_{F,\tau}(r)$. Several prescriptions are possible for the local density ρ in $g^D_{\tau\tau'}$ and $g^E_{\tau\tau'}$. In the present calculations, the midpoint prescription is employed:

$$\rho=\sum_\tau\rho_\tau(\boldsymbol{r}_m). \tag{5}$$

In the G-matrix folding approach presented in Ref. [9], energy- and density-dependent effective interactions in spin-singlet even, spin-triplet even, spin-singlet odd, and spin-triplet odd states are parametrized in a three-range local Gaussian form in coordinate space.

In the improved LDA method, the single-particle potential in nuclear matter is assigned to the potential at the corresponding density in a finite nucleus. The single-particle potential $U_{NM}(k;\rho)$ as a function of momentum k in nuclear matter having the density $\rho=\frac{2}{3\pi^2}k^3_F$ with the Fermi momentum k_F is converted to the potential $U_{NM}(E;\rho)$ as a function of the energy E through the relation

$$E=\frac{\hbar^2}{2m}k^2+U_{NM}(k;\rho). \tag{6}$$

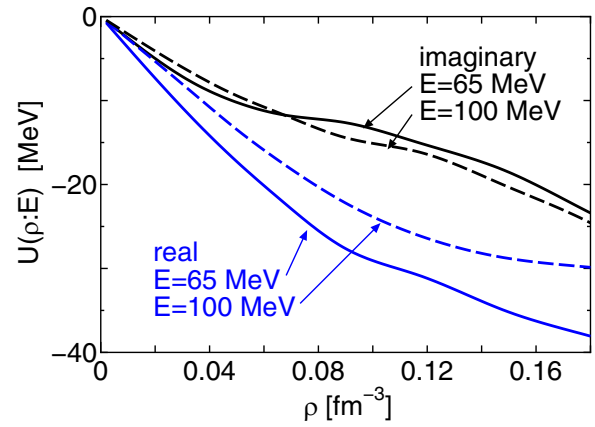

FIG. 1. Density dependence of the single-particle potential in nuclear matter when the nucleon energy E is specified.

The complex nuclear matter potential $U_{NM}(k;\rho)$ is the result of the G-matrix calculations [15] using nucleon-nucleon interactions of chiral effective field theory with incorporating the effects of three-nucleon forces.

Some details are noted for the G-matrix calculations. In solving the G-matrix equation, the so-called continuous choice is employed for the intermediate spectra. Without using an effective approximation, namely a parabolic approximation, the single-particle potential is interpolated in terms of the values at mesh points. It has been known that the Brueckner self-consistent calculation does not converge at low densities, namely at $k_F\lesssim 0.8$ fm^{-1} or $\rho\lesssim 0.2\rho_0$ with ρ_0 being the normal density, probably due to the onset of clustering of nuclear matter. When the density is 0.2–0.55 fm^{-3}, converging results are obtained. However, the potential self-consistently determined bears problematic wavy behavior between $k=1$ fm and $k=3$ fm, presumably as the precursor of the clustering. Such behavior brings about peculiar density dependence especially in the imaginary part of the single-particle potential, which is irrelevant in finite nuclei. Because the G-matrix equation for scattering states is the method to deal with high-momentum singularities of NN interactions, a smooth single-particle potential is better to be used in the intermediate spectra. The practical way of smoothing or averaging the potential is to reduce the number of mesh points for the self-consistent determination of the potential. This prescription hardly changes the single-particle potential at $k\lesssim 1$ fm and $k\gtrsim 3$ fm. The single-particle potential applied to the low-density region below $0.2\rho_0$ is estimated by the interpolation as a function of the density between zero at $\rho=0$ and those above $\rho=0.2$ fm^{-3}. The obtained complex potentials $U_{NM}(E;\rho)$ are shown in Fig. 1 as a function of the density ρ at the energies $E=65$ and 100 MeV.

The OMP $U(r)$ in a finite nucleus having the density profile $\rho(r)$ is constructed as

$$U(r;E)=U_{NM}(E;\rho(r)). \tag{7}$$

To correct the finite-range effects, a Gaussian form factor is introduced.

$$U(r;E)=(\sqrt{\pi}\beta)^{-3}\int d\boldsymbol{r}'e^{-[(\boldsymbol{r}-\boldsymbol{r}')/\beta]^2}U_{NM}(E;\rho(r')). \tag{8}$$

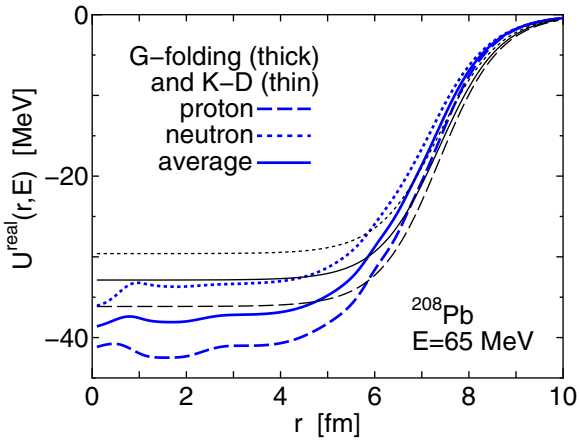

FIG. 2. Proton, neutron, and average OMPs in ^{208}Pb at the energy $E = 65$ MeV. The thick curves represent the potentials obtained by the G-matrix folding method in Ref. [9]. The thin curves are phenomenological potentials in a Woods-Saxon form parametrized by Koning and Delaroche [16].

In the present improved LDA calculations, single-particle potentials in symmetric nuclear matter are considered. Therefore, there is no difference between the proton and neutron potentials. In finite nuclei, however, the proton and neutron OMPs are generally different due to the different proton and neutron density distributions and the isospin-dependence

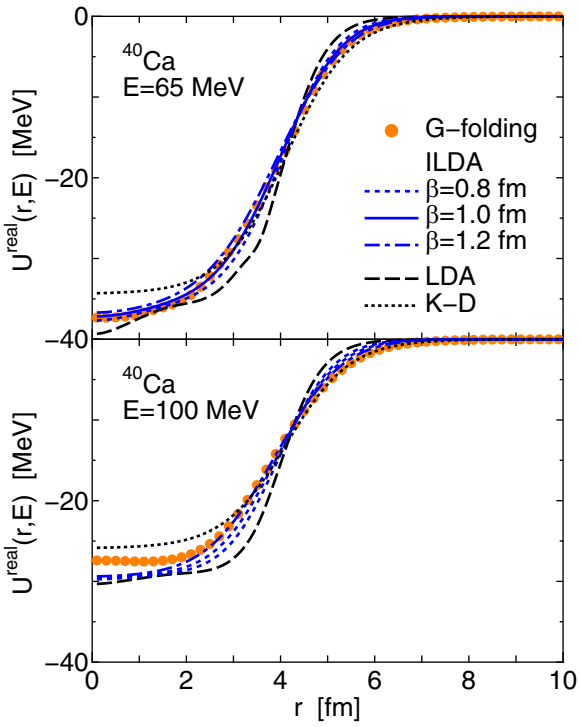

FIG. 3. LDA and improved LDA OMPs in the real part for ^{40}Ca at $E = 65$ and 100 MeV are compared with the proton-neutron average potential calculated by the G-matrix folding method. The proton-neutron average Woods-Saxon OMPs by Koning and Delaroche [16] are also shown by the dotted curves.

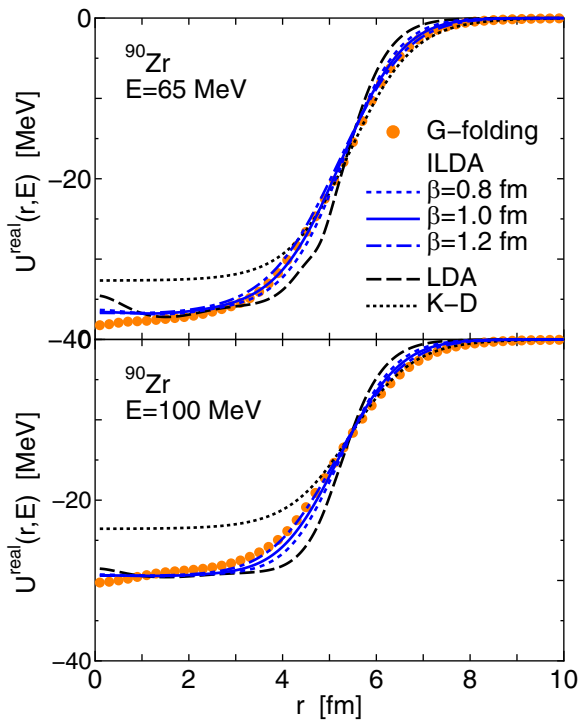

FIG. 4. Same as Fig. 3, but for ^{90}Zr.

of the interactions. To compare the calculated OMPs in the improved LDA method with those from the G-matrix folding method and also with the phenomenological OMPs, the average of the proton and neutron OMPs is considered. The proton, neutron, and average OMPs in ^{208}Pb at the energy $E = 65$ MeV are demonstrated in Fig. 2 both for the phenomenological Woods-Saxon parametrization by Koning and Delaroche [16] and the G-matrix folding method. The Woods-Saxon potentials are shallower than those of the G-matrix folding method. The difference can be explained by the second-order Pauli rearrangement contribution [10], which is not taken into account in the latter potential.

A. Real part

Microscopic OMPs are calculated in the G-matrix folding method and the improved LDA method for ^{40}Ca, ^{90}Zr, and ^{208}Pb at the energies $E = 65$ and 100 MeV, using the G matrices [15] of chiral nucleon-nucleon interactions with effects of three-nucleon forces. Density distributions of the target nuclei are provided by Hartree-Fock single-particle wave functions with the Gogny D1S effective force [17]. Results are presented in Figs. 3, 4, and 5. Representative empirical Woods-Saxon potentials by Koning and Delaroche [16] are also included. Besides, the potentials by the simple LDA method are shown for comparison.

The steep slope of the OMP in the surface area by the simple LDA method moderates in the improved LDA method. The range parameter of around $\beta = 1$ fm reproduces well the OMP of the G-matrix folding method. These microscopic potentials also show good correspondence to the phenomenological Woods-Saxon potential, except for the difference in

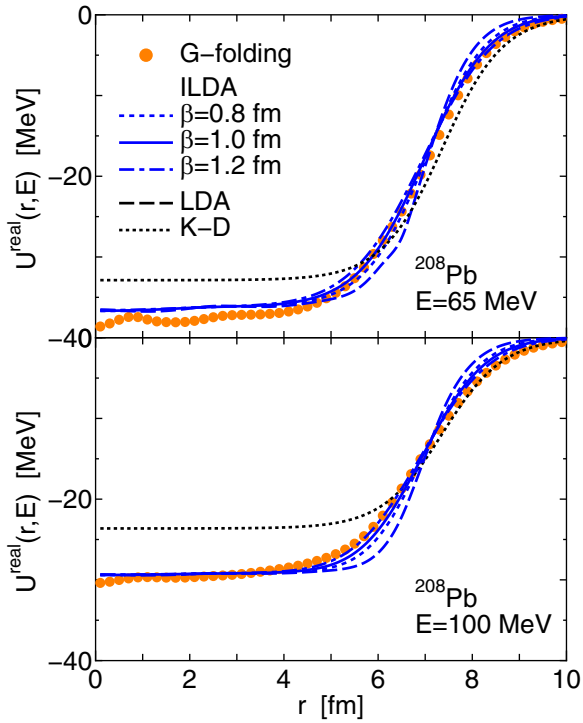

FIG. 5. Same as Fig. 3, but for ^{208}Pb.

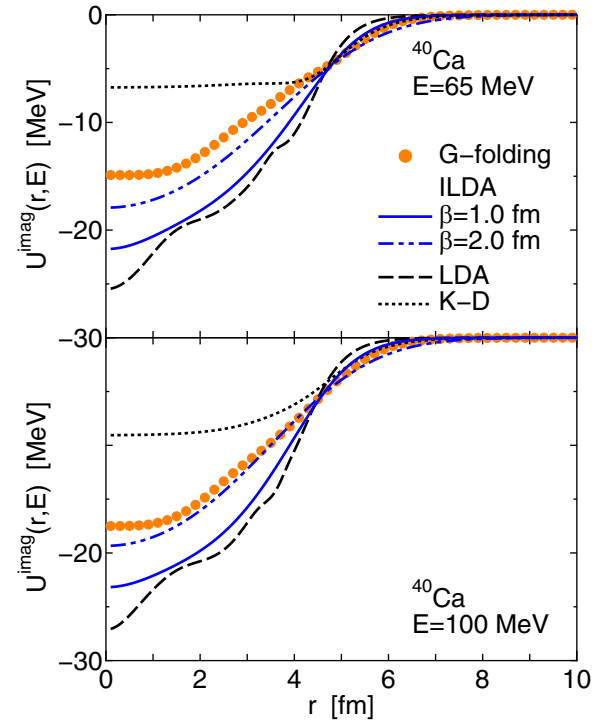

FIG. 6. LDA and improved LDA OMPs in the imaginary part for ^{40}Ca at $E = 65$ and 100 MeV are compared with the proton-neutron average potential calculated by the G-matrix folding method. The Woods-Saxon OMPs by Koning and Delaroche [16] are also shown.

the central region. The difference between the Koning and Delaroche potential and the G-matrix folding potential in a real part is of the order of the rearrangement potential [10] which is absent in the lowest order G-matrix folding potential.

B. Imaginary part

The comparison between the G-matrix folding method and the improved LDA method is also made for the imaginary part of the microscopic OMP in Figs. 6, 7, and 8. The results of the simple LDA are also shown by the dashed curves. The imaginary strength of the improved LDA method in the central region is larger than that of the G-matrix folding method, though the calculations are based on the same G matrices in nuclear matter. Comparing to these microscopic imaginary potentials, the phenomenological Koning and Delaroche imaginary potential is much shallower in the inner region.

The second-order rearrangement effect, which brings about repulsive contributions [10] to fill the difference between the lowest-order microscopic real part and the phenomenological real part, does not contribute to an imaginary part. Any higher-order process cannot provide a positive contribution to the imaginary potential and therefore does not solve the discrepancy. The overestimation of the microscopic OMP in the imaginary strength may be attributed to the continuum level density near the Fermi surface in nuclear matter [18]. It is also possible that the nonlocal imaginary G-matrix elements may not be well simulated in a convenient local-function form. To remedy the overestimation, a renormalization factor is sometimes introduced. For example, the reduction factor in Ref. [8] is $0.65 \approx 0.8$, depending on the bare nucleon-nucleon interaction employed. On the other hand, microscopic

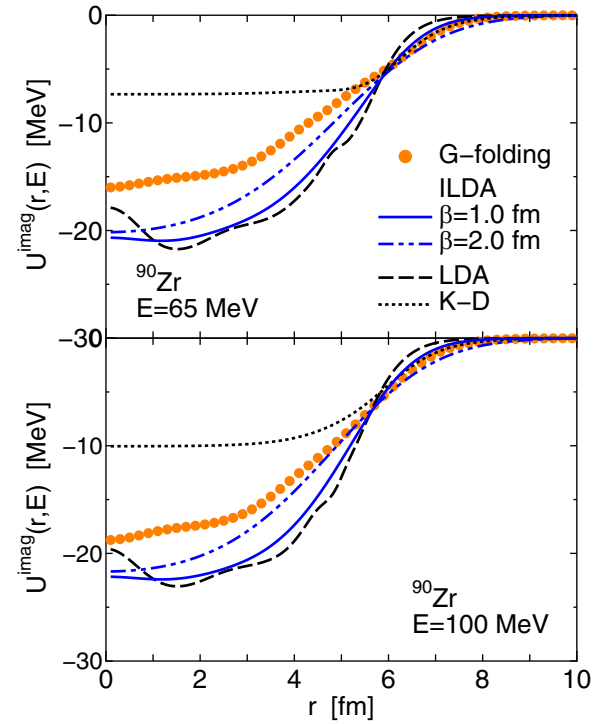

FIG. 7. Same as Fig. 6, but for ^{90}Zr.

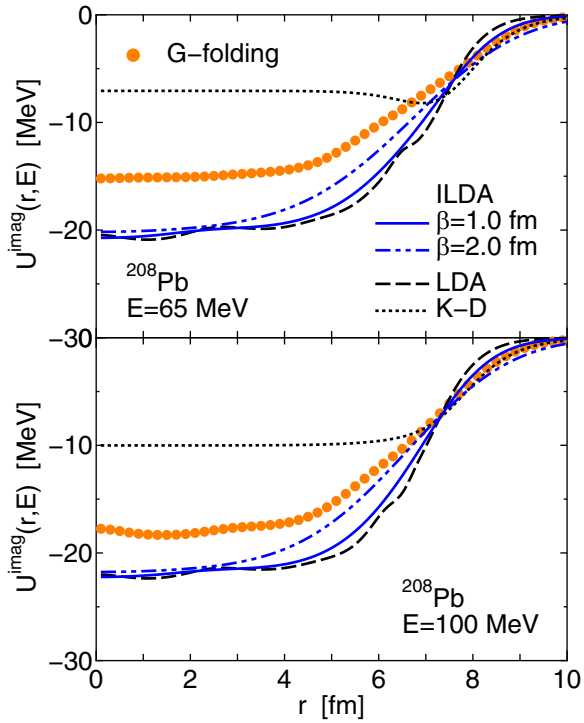

FIG. 8. Same as Fig. 6, but for ^{208}Pb.

calculations of the proton elastic scattering on ^{40}Ca, ^{58}Ni, and ^{208}Pb reported in Ref. [19] using the G matrices in Ref. [9], on which the present paper is based, do not include the renormalization factor. In the OMP in Ref. [19], the imaginary potential is deeper than that of the phenomenological potential, as is shown in Figs. 6–8. This difference, however, does not influence much the description of nucleon elastic scattering on nuclei when the nucleon incident energy is not high, as far as the complex OMP is similar in the surface area. This point is demonstrated in Sec. II C.

C. Differential cross section

The OMPs of the improved LDA method and the G-matrix folding method are similar in the real part, but show some difference in the imaginary part in the inner region. The phenomenological Koning and Delaroche potential is shallower in the inner region than the microscopic potentials both in the real and imaginary parts. It is instructive to see how different results are obtained when differential cross sections of elastic scattering are calculated with these OMPs.

Figures 9–11 represent angular distributions of proton elastic scattering on ^{40}Ca at the energies $E = 65$ MeV and $E = 100$ MeV calculated by the four sets of the proton-neutron average OMP. Experimental data available at $E = 65$ MeV [20,21] are included. The results of the phenomenological Koning and Delaroche Woods-Saxon potential, the real and imaginary potentials of which are depicted in Figs. 3–8 by the dotted curves, are shown by the small circles in a row. The cross sections obtained with the proton-neutron average G-matrix folding potential are shown by the solid curve. When the real part of the G-matrix folding potential is replaced

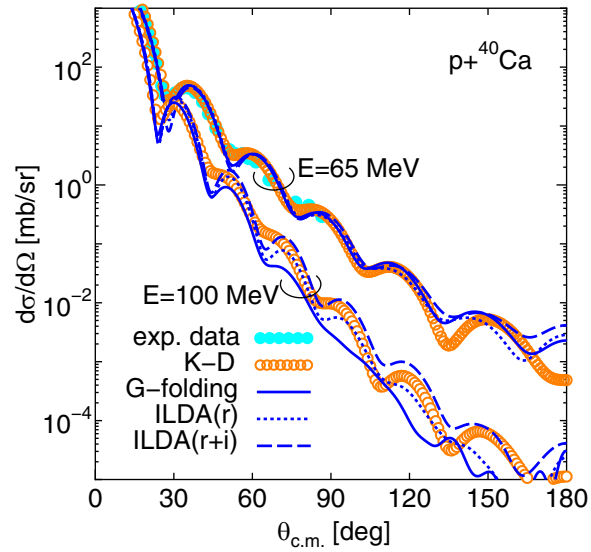

FIG. 9. Differential cross sections of proton scattering on ^{40}Ca at the energy $E = 65$ MeV calculated by proton-neutron average OMPs. The small circles in a row denote the result of the phenomenological Woods-Saxon potential by Koning and Delaroche [16]. The solid curve represents the result of the G-matrix folding calculation. The dotted curve shows the result of the potential in which the real part of the G-folding potential is replaced by the improved LDA potential with $\beta = 1.0$ fm. The improved LDA potential supplemented by the spin-orbit potential of the G-matrix folding potential gives the dashed curve. Experimental data at $E = 65$ MeV are taken from Ref. [20].

by that of the improved LDA method, the dotted curve is obtained. Finally, the improved LDA potential supplemented by the spin-orbit potential of the G-matrix folding method gives the dashed curve. The four results are close to each other at $E = 65$ MeV except for the backward angles and account

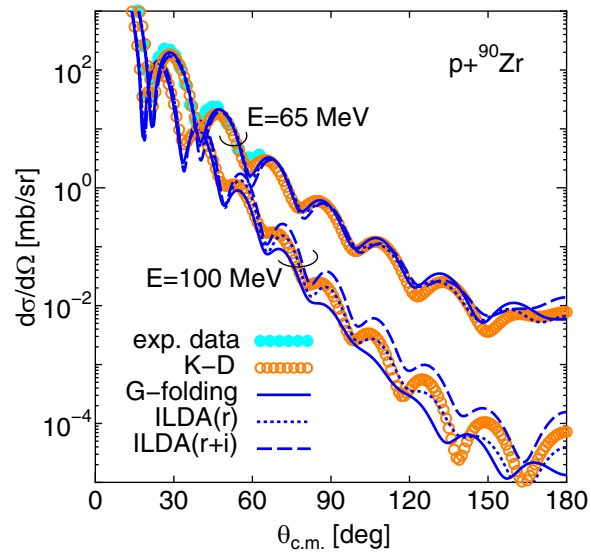

FIG. 10. Same as Fig. 9, but for ^{90}Zr. Experimental data at $E = 65$ MeV are taken from Ref. [21].

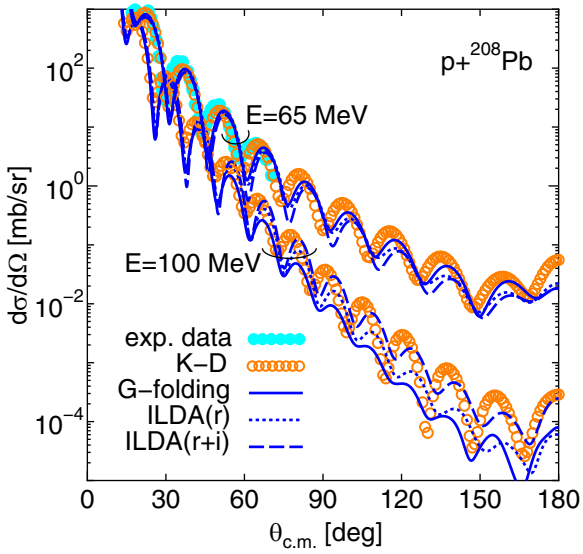

FIG. 11. Same as Fig. 9, but for ^{208}Pb. Experimental data at $E = 65$ MeV are taken from Ref. [20].

well for experimental data, although the potential strength in particular in the imaginary part is varying as is seen in Fig. 6–8. This result indicates that the nucleon elastic scattering on nuclei at this energy is determined almost by the properties of the OMP in the surface area and therefore is insensitive to the strength in the inner region. At $E = 100$ MeV, the influence of the inner part of the OMP increases and the differences among the four results become larger.

The real part of the microscopic OMP is very similar to the phenomenological one, especially the second-order Pauli rearrangement contribution is included. On the other hand, the imaginary part shows a variation. As noted in Sec. II B, there is some problem in the nuclear matter approach. There should be further investigations for the microscopic understanding of the optical-model imaginary potential in nuclei. It is also an interesting subject to study whether the difference of the OMP in the central region can be checked in other applications such as the description of inelastic processes or not.

III. THEORETICAL CONSIDERATION

It is worthwhile to consider the reason behind the good agreement of the real part of the OMP calculated by the improved LDA method with that by the more involved G-matrix folding method. In this section, it is shown that the Gaussian folded LDA expression is obtained starting from a general definition of the microscopic OMP by introducing several reasonable approximations and assumptions.

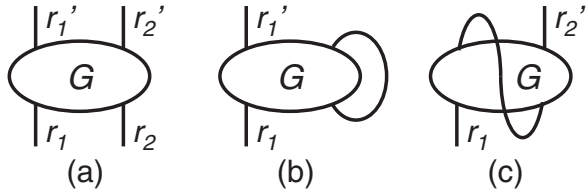

FIG. 12. Nonlocal interaction G and its folding by single-particle states.

Suppose that the two-body G matrix is given in nuclear matter as $G(\boldsymbol{k}', \boldsymbol{k}; \boldsymbol{K}, \omega)$, which generally depends on the initial and final relative momenta ($\boldsymbol{k}$ and $\boldsymbol{k}'$), the center-of-mass momentum $\boldsymbol{K}$ and the starting energy ω of the interacting two nucleons. The matrix element in momentum space is transformed into a nonlocal two-body interaction in coordinate space, Fig. 12(a), as

$$G^{S,T}(\boldsymbol{r}_1', \boldsymbol{r}_2', \boldsymbol{r}_1, \boldsymbol{r}_2) = \frac{(2\pi)^3}{(2\pi)^{12}} \iiiint d\boldsymbol{k}_1' d\boldsymbol{k}_2' d\boldsymbol{k}_1 d\boldsymbol{k}_2 \times e^{i(\boldsymbol{k}_1'\cdot\boldsymbol{r}_1' + \boldsymbol{k}_2'\cdot\boldsymbol{r}_2' - \boldsymbol{k}_1\cdot\boldsymbol{r}_1 - \boldsymbol{k}_2\cdot\boldsymbol{r}_2)} \times G^{S,T}(\boldsymbol{k}', \boldsymbol{k}; \boldsymbol{K}, \omega)\delta(\boldsymbol{K}' - \boldsymbol{K}), \quad (9)$$

where $\boldsymbol{k}_1' = \frac{1}{2}\boldsymbol{K}' + \boldsymbol{k}'$, $\boldsymbol{k}_2' = \frac{1}{2}\boldsymbol{K}' - \boldsymbol{k}'$, $\boldsymbol{k}_1 = \frac{1}{2}\boldsymbol{K} + \boldsymbol{k}$, and $\boldsymbol{k}_2 = \frac{1}{2}\boldsymbol{K} - \boldsymbol{k}$. A one-body nonlocal potential is constructed by folding the G matrix by occupied state wave functions $\phi_h(\boldsymbol{r})$ of a finite nucleus. The coordinate system is now referred to by the center of the nucleus. First, a direct contribution from the convolution by $\phi_h^*(\boldsymbol{r}_2')\phi_h(\boldsymbol{r}_2)$ is considered, and next an exchange contribution from the convolution by $-\phi_h^*(\boldsymbol{r}_1')\phi_h(\boldsymbol{r}_2)$ is considered.

A. Direct term

The direct contribution, Fig. 12(b), is given by

$$\begin{aligned} U_D(\boldsymbol{r}_1', \boldsymbol{r}_1) &= \sum_h \iint d\boldsymbol{r}_2' d\boldsymbol{r}_2 G(\boldsymbol{r}_1', \boldsymbol{r}_2', \boldsymbol{r}_1, \boldsymbol{r}_2)\phi_h^*(\boldsymbol{r}_2')\phi_h(\boldsymbol{r}_2) \\ &= \sum_h \iint d\boldsymbol{r}_2' d\boldsymbol{r}_2 \frac{(2\pi)^3}{(2\pi)^{12}} \iiiint d\boldsymbol{k}_1' d\boldsymbol{k}_2' d\boldsymbol{k}_1 d\boldsymbol{k}_2 \\ &\quad \times e^{i(\boldsymbol{k}_1'\cdot\boldsymbol{r}_1' + \boldsymbol{k}_2'\cdot\boldsymbol{r}_2' - \boldsymbol{k}_1\cdot\boldsymbol{r}_1 - \boldsymbol{k}_2\cdot\boldsymbol{r}_2)}\delta(\boldsymbol{K}' - \boldsymbol{K}) \\ &\quad \times \sum_{S,T} \hat{S}\hat{T} G^{S,T}(\boldsymbol{k}', \boldsymbol{k}; \boldsymbol{K}, \omega)\phi_h^*(\boldsymbol{r}_2')\phi_h(\boldsymbol{r}_2). \end{aligned} \quad (10)$$

The nucleus is assumed to be spherical, and the Slater approximation of the density-matrix expansion [13,14] is introduced:

$$\sum_h \phi_h^*(\boldsymbol{r}_2')\phi_h(\boldsymbol{r}_2) \simeq \rho(R_2)\frac{3}{s_2 k_F(R_2)} j_1(s_2 k_F(R_2)), \quad (11)$$

where $\boldsymbol{R}_2 = \frac{1}{2}(\boldsymbol{r}_2' + \boldsymbol{r}_2)$ and $\boldsymbol{s}_2 = \boldsymbol{r}_2 - \boldsymbol{r}_2'$. j_1 is a spherical Bessel function of the first kind and $k_F(R)$ is a local Fermi momentum relating to a local density $\rho(R)$ by $\rho(R) = \frac{2}{3\pi^2}k_F^3(R)$. Introducing $\boldsymbol{R}_1 = \frac{1}{2}(\boldsymbol{r}_1' + \boldsymbol{r}_1)$ and $\boldsymbol{s}_1 = \boldsymbol{r}_1 - \boldsymbol{r}_1'$, and noticing $\boldsymbol{K}' = \boldsymbol{K}$, the exponent in Eq. (2) is rewritten as

$$\begin{aligned} &\boldsymbol{k}_1'\cdot\boldsymbol{r}_1' + \boldsymbol{k}_2'\cdot\boldsymbol{r}_2' - \boldsymbol{k}_1\cdot\boldsymbol{r}_1 - \boldsymbol{k}_2\cdot\boldsymbol{r}_2 \\ &= (\boldsymbol{k}_1' - \boldsymbol{k}_1)\cdot\boldsymbol{R}_1 - (\boldsymbol{k}' - \boldsymbol{k})\cdot\boldsymbol{R}_2 \\ &\quad - \tfrac{1}{2}(\boldsymbol{K} + \boldsymbol{k}' + \boldsymbol{k})\cdot\boldsymbol{s}_1 - \tfrac{1}{2}(\boldsymbol{K} - \boldsymbol{k}' - \boldsymbol{k})\cdot\boldsymbol{s}_2. \end{aligned} \quad (12)$$

The above change of the variables leads to

$$U_D(\boldsymbol{r}_1', \boldsymbol{r}_1) = U\left(\boldsymbol{R}_1 - \frac{1}{2}\boldsymbol{s}_1, \boldsymbol{R}_1 + \frac{1}{2}\boldsymbol{s}_1\right) \simeq \iint d\boldsymbol{R}_2 d\boldsymbol{s}_2\ \rho(R_2)\frac{3}{s_2 k_F(R_2)} j_1(s_2 k_F(R_2))\frac{1}{(2\pi)^9}\iiint d\boldsymbol{K} d\boldsymbol{k}' d\boldsymbol{k} \sum_{S,T}\hat{S}\hat{T}$$
$$\times G^{S,T}(\boldsymbol{k}', \boldsymbol{k}; \boldsymbol{K}, \omega) e^{i\{(\boldsymbol{k}'-\boldsymbol{k})\cdot\boldsymbol{R}_1 - (\boldsymbol{k}'-\boldsymbol{k})\cdot\boldsymbol{R}_2\}} e^{i\{-\frac{1}{2}(\boldsymbol{K}+\boldsymbol{k}'+\boldsymbol{k})\cdot\boldsymbol{s}_1 - \frac{1}{2}(\boldsymbol{K}-\boldsymbol{k}'-\boldsymbol{k})\cdot\boldsymbol{s}_2\}}. \tag{13}$$

Using the following integration formula:[1]

$$\int d\boldsymbol{x} e^{i\boldsymbol{q}\cdot\boldsymbol{x}} \frac{3}{x k_F} j_1(k_F x) = \frac{6\pi^2}{k_F^3}\theta(k_F - q), \tag{14}$$

where $\theta(x)$ is a step function, and carrying out the angle integration of $d\boldsymbol{R}_2$

$$\int d\Omega_2 e^{-i(\boldsymbol{k}'-\boldsymbol{k})\cdot\boldsymbol{R}_2} = 4\pi\, j_0(|\boldsymbol{k}' - \boldsymbol{k}|R_2), \tag{15}$$

the nonlocal potential $U_D(\boldsymbol{r}_1', \boldsymbol{r}_1)$ becomes

$$U_D(\boldsymbol{r}_1', \boldsymbol{r}_1) = U\left(\boldsymbol{R}_1 - \frac{1}{2}\boldsymbol{s}_1, \boldsymbol{R}_1 + \frac{1}{2}\boldsymbol{s}_1\right) \simeq \int 4\pi R_2^2 dR_2\ \frac{4}{(2\pi)^9}\iiint d\boldsymbol{K} d\boldsymbol{k}' d\boldsymbol{k} e^{i((\boldsymbol{k}'-\boldsymbol{k})\cdot\boldsymbol{R}_1 - \frac{1}{2}(\boldsymbol{K}+\boldsymbol{k}'+\boldsymbol{k})\cdot\boldsymbol{s}_1} \sum_{S,T}\hat{S}\hat{T}$$
$$\times G^{S,T}(\boldsymbol{k}', \boldsymbol{k}; \boldsymbol{K}, \omega) j_0(|\boldsymbol{k}' - \boldsymbol{k}|R_2)\theta\left(k_F(R_2) - \frac{1}{2}|\boldsymbol{K} - \boldsymbol{k}' - \boldsymbol{k}|\right). \tag{16}$$

To localize the nonlocal potential $U_D(\boldsymbol{r}_1', \boldsymbol{r}_2')$, a WKB method [22] is employed. Namely, a Wigner transformation is operated on $U_D(\boldsymbol{r}_1', \boldsymbol{r}_2')$

$$U_D(\boldsymbol{R}_1, \boldsymbol{p}) \equiv \int d\boldsymbol{s}_1 e^{i\boldsymbol{p}\cdot\boldsymbol{s}_1} U_D\left(\boldsymbol{R}_1 - \frac{1}{2}\boldsymbol{s}_1, \boldsymbol{R}_1 + \frac{1}{2}\boldsymbol{s}_1\right), \tag{17}$$

and $\boldsymbol{p}$ is set to be a momentum that satisfies local energy conservation

$$E = \frac{\hbar^2}{2m}\boldsymbol{p}^2 + U(\boldsymbol{R}_1, \boldsymbol{p}). \tag{18}$$

The spherical symmetry allows an angle average $\frac{1}{4\pi}\int d\Omega_1$, by which $e^{i(\boldsymbol{k}'-\boldsymbol{k})\cdot\boldsymbol{R}_1}$ is replaced by $j_0(|\boldsymbol{k}' - \boldsymbol{k}|R_1)$. Then,

$$\begin{aligned} U_D(\boldsymbol{R}_1, \boldsymbol{p}) &= \int d\boldsymbol{s}_1 e^{i\boldsymbol{p}\cdot\boldsymbol{s}_1}\int 4\pi R_2^2 dR_2 \frac{4}{(2\pi)^9}\iiint d\boldsymbol{K} d\boldsymbol{k}' d\boldsymbol{k}\ \sum_{S,T}\hat{S}\hat{T} G^{S,T}(\boldsymbol{k}', \boldsymbol{k}; \boldsymbol{K}, \omega) \\ &\quad\times\theta\left(k_F(R_2) - \frac{1}{2}|\boldsymbol{K} - \boldsymbol{k}' - \boldsymbol{k}|\right) j_0(|\boldsymbol{k}' - \boldsymbol{k}|R_2) j_0(|\boldsymbol{k}' - \boldsymbol{k}|R_1) e^{-i\frac{1}{2}(\boldsymbol{K}+\boldsymbol{k}'+\boldsymbol{k})\cdot\boldsymbol{s}_1} \\ &= \int 4\pi R_2^2 dR_2\ \frac{4\times 2^3}{(2\pi)^6}\iint d\boldsymbol{k}' d\boldsymbol{k}\ \sum_{S,T}\hat{S}\hat{T} G^{S,T}(\boldsymbol{k}', \boldsymbol{k}; \boldsymbol{K} = 2\boldsymbol{p} - \boldsymbol{k}' - \boldsymbol{k}, \omega) \\ &\quad\times\theta(k_F(R_2) - |\boldsymbol{p} - \boldsymbol{k}' - \boldsymbol{k}|) j_0(|\boldsymbol{k}' - \boldsymbol{k}|R_2) j_0(|\boldsymbol{k}' - \boldsymbol{k}|R_1). \end{aligned} \tag{19}$$

Applying the change of variables $\boldsymbol{x} = \boldsymbol{k} - \boldsymbol{k}'$ and $\boldsymbol{q} = \frac{1}{2}(\boldsymbol{k}' + \boldsymbol{k})$,

$$U_D(\boldsymbol{R}_1, \boldsymbol{p}) = \int 4\pi R_2^2 dR_2\ \frac{4\times 2^3}{(2\pi)^6}\iint d\boldsymbol{x} d\boldsymbol{q}\ \sum_{S,T}\hat{S}\hat{T} G^{S,T}\left(\boldsymbol{q} - \frac{1}{2}\boldsymbol{x}, \boldsymbol{q} + \frac{1}{2}\boldsymbol{x}; \boldsymbol{K} = 2\boldsymbol{p} - 2\boldsymbol{q}, \omega\right)$$
$$\times\theta(k_F(R_2) - |\boldsymbol{p} - 2\boldsymbol{q}|) j_0(xR_2) j_0(xR_1). \tag{20}$$

[1]Note that $\theta(k_F - q)$ should be $1/2$ when $q = k_F$.

B. Exchange term

The exchange contribution, Fig. 12(c), namely the convolution of the two-body G matrix by $-\phi_h^*(\boldsymbol{r}_1')\phi_h(\boldsymbol{r}_2)$, is also treated in the same manner.

$$\begin{aligned} U_E(\boldsymbol{r}_2', \boldsymbol{r}_1) &= -\sum_h \iint d\boldsymbol{r}_1' d\boldsymbol{r}_2 G(\boldsymbol{r}_1', \boldsymbol{r}_2', \boldsymbol{r}_1, \boldsymbol{r}_2)\phi_h^*(\boldsymbol{r}_1')\phi_h(\boldsymbol{r}_2) \\ &= -\sum_h \iint d\boldsymbol{r}_1' d\boldsymbol{r}_2 \frac{(2\pi)^3}{(2\pi)^{12}} \iiint\!\!\iint d\boldsymbol{k}_1' d\boldsymbol{k}_2' d\boldsymbol{k}_1 d\boldsymbol{k}_2 e^{i(\boldsymbol{k}_1'\cdot\boldsymbol{r}_1' + \boldsymbol{k}_2'\cdot\boldsymbol{r}_2' - \boldsymbol{k}_1\cdot\boldsymbol{r}_1 - \boldsymbol{k}_2\cdot\boldsymbol{r}_2)} \\ &\quad \times \sum_{S,T}(-1)^{S+T}\hat{S}\hat{T}G^{S,T}(\boldsymbol{k}', \boldsymbol{k}; \boldsymbol{K}, \omega)\delta(\boldsymbol{K}' - \boldsymbol{K})\phi_h^*(\boldsymbol{r}_1')\phi_h(\boldsymbol{r}_2). \end{aligned} \tag{21}$$

This time, $\boldsymbol{R}_2 = \frac{1}{2}(\boldsymbol{r}_1' + \boldsymbol{r}_2)$ and $\boldsymbol{s}_2 = \boldsymbol{r}_2 - \boldsymbol{r}_1'$ are defined. Again, the Slater approximation in the density-matrix expansion is introduced for the nonlocal density.

$$\sum_h \phi_h^*(\boldsymbol{r}_1')\phi_h(\boldsymbol{r}_2) \simeq \rho(R_2)\frac{3}{s_2 k_F(R_2)} j_1(s_2 k_F(R_2)). \tag{22}$$

Similar manipulation as before leads to

$$\begin{aligned} U_E(\boldsymbol{r}_2', \boldsymbol{r}_1) = U_E\left(\boldsymbol{R}_1 - \frac{1}{2}\boldsymbol{s}_1, \boldsymbol{R}_1 + \frac{1}{2}\boldsymbol{s}_1\right) &\simeq -\iint 4\pi R_2^2 dR_2 \frac{4}{(2\pi)^9} \iiint d\boldsymbol{K} d\boldsymbol{k}' d\boldsymbol{k} e^{i((\boldsymbol{k}'-\boldsymbol{k})\cdot\boldsymbol{R}_1 - (\boldsymbol{k}'-\boldsymbol{k})\cdot\boldsymbol{R}_2 - \frac{1}{2}(\boldsymbol{K}+\boldsymbol{k}'+\boldsymbol{k})\cdot\boldsymbol{s}_1} \\ &\quad \times \sum_{S,T}(-1)^{S+T}\hat{S}\hat{T}G^{S,T}(-\boldsymbol{k}', \boldsymbol{k}; \boldsymbol{K}, \omega) j_0(|\boldsymbol{k}' - \boldsymbol{k}|R_2)\theta\left(k_F(R_2) - \frac{1}{2}|\boldsymbol{K} - \boldsymbol{k}' - \boldsymbol{k}|\right). \end{aligned} \tag{23}$$

The only difference of this expression from that of the direct contribution, Eq. (8), is in $G(-\boldsymbol{k}', \boldsymbol{k}; \boldsymbol{K}, \omega)$, except for the overall negative sign. The WKB localization is again performed on $U_E(\boldsymbol{R}_1 - \frac{1}{2}\boldsymbol{s}_1, \boldsymbol{R}_1 + \frac{1}{2}\boldsymbol{s}_1)$ to give $U_E(\boldsymbol{R}_1, \boldsymbol{p})$.

C. Sum of the direct and exchange contributions

The sum of the direct and exchange contributions reads

$$\begin{aligned} U(\boldsymbol{R}_1, \boldsymbol{p}) = U_D(\boldsymbol{R}_1, \boldsymbol{p}) + U_E(\boldsymbol{R}_1, \boldsymbol{p}) &= \int 4\pi R_2^2 dR_2 \frac{4\times 2^3}{(2\pi)^6} \iint d\boldsymbol{x} d\boldsymbol{q} \sum_{S,T}\hat{S}\hat{T}\left\{G^{S,T}\left(\boldsymbol{q} - \frac{1}{2}\boldsymbol{x}, \boldsymbol{q} + \frac{1}{2}\boldsymbol{x}; \boldsymbol{K} = 2\boldsymbol{p} - 2\boldsymbol{q}, \omega\right)\right. \\ &\left. - (-1)^{S+T}G^{S,T}\left(-\boldsymbol{q} + \frac{1}{2}\boldsymbol{x}, \boldsymbol{q} + \frac{1}{2}\boldsymbol{x}; \boldsymbol{K} = 2\boldsymbol{p} - 2\boldsymbol{q}, \omega\right)\right\}\theta(k_F(R_2) - |\boldsymbol{p} - 2\boldsymbol{q}|) j_0(xR_2) j_0(xR_1). \end{aligned} \tag{24}$$

Let us recall the definition of the lowest-order single-particle potential $U_{NM}(\boldsymbol{p})$ in nuclear matter with the Fermi momentum k_F, which is given by the sum of direct and exchange contributions

$$\begin{aligned} U_{NM}(\boldsymbol{p}; k_F) = \sum_{\boldsymbol{h}'}\langle \boldsymbol{p}\boldsymbol{h}'|G|\boldsymbol{p}\boldsymbol{h}' - \boldsymbol{h}'\boldsymbol{p}\rangle\theta(k_F - |\boldsymbol{h}'|) &= \frac{1}{(2\pi)^3}\int 2^3 d\boldsymbol{q} \sum_{S,T}\hat{S}\hat{T}\{G^{S,T}(\boldsymbol{q}, \boldsymbol{q}; \boldsymbol{K} = 2\boldsymbol{p} - 2\boldsymbol{q}, \omega) \\ &\quad - (-1)^{S+T}G^{S,T}(-\boldsymbol{q}, \boldsymbol{q}; \boldsymbol{K} = 2\boldsymbol{p} - 2\boldsymbol{q}, \omega)\}\theta(k_F - |\boldsymbol{p} - 2\boldsymbol{q}|), \end{aligned} \tag{25}$$

where the relative momentum $\boldsymbol{q} = \frac{1}{2}(\boldsymbol{p} - \boldsymbol{h}')$ is introduced.

Now, the following factorization is postulated for G:

$$\begin{aligned} &G^{S,T}\left(\boldsymbol{q} - \frac{1}{2}\boldsymbol{x}, \boldsymbol{q} + \frac{1}{2}\boldsymbol{x}; \boldsymbol{K} = 2\boldsymbol{p} - 2\boldsymbol{q}, \omega\right) - (-1)^{S+T}G^{S,T}\left(-\boldsymbol{q} + \frac{1}{2}\boldsymbol{x}, \boldsymbol{q} + \frac{1}{2}\boldsymbol{x}; \boldsymbol{K} = 2\boldsymbol{p} - 2\boldsymbol{q}, \omega\right) \\ &\simeq e^{-(\mu\boldsymbol{x}/2)^2}\{G^{S,T}(\boldsymbol{q}, \boldsymbol{q}; \boldsymbol{K} = 2\boldsymbol{p} - 2\boldsymbol{q}, \omega) - (-1)^{S+T}G^{S,T}(-\boldsymbol{q}, \boldsymbol{q}; \boldsymbol{K} = 2\boldsymbol{p} - 2\boldsymbol{q}, \omega)\}. \end{aligned} \tag{26}$$

Then,

$$U(\boldsymbol{R}_1, \boldsymbol{p}) = \int 4\pi R_2^2 dR_2 \frac{1}{(2\pi)^3}\int d\boldsymbol{x}\frac{1}{8}U_{NM}(\boldsymbol{p}; k_F(R_2))e^{-(\mu\boldsymbol{x}/2)^2} j_0(xR_2) j_0(xR_1). \tag{27}$$

This $d\boldsymbol{x}$ integration is carried out analytically:

$$\int d\boldsymbol{x}\, e^{-\frac{\mu^2 x^2}{4}} j_0(R_1 x) j_0(R_2 x) = \frac{4\pi}{2R_1R_2}\frac{\sqrt{\pi}}{\mu}\left(e^{-\frac{1}{\mu^2}(R_1 - R_2)^2} - e^{-\frac{1}{\mu^2}(R_1 + R_2)^2}\right). \tag{28}$$

It is easy to see that the right-hand side can be expressed in the following form:

$$\int d\boldsymbol{x}\, e^{-\frac{\mu^2 x^2}{4}} j_0(R_1 x) j_0(R_2 x) = \frac{4(\sqrt{\pi})^3}{\mu^3} \int_{-1}^{1} d\cos\theta\; e^{-\frac{1}{\mu^2}(\boldsymbol{R}_1 - \boldsymbol{R}_2)^2}, \tag{29}$$

where $\cos\theta = \boldsymbol{R}_1 \cdot \boldsymbol{R}_2/(R_1 R_2)$. Therefore, the following expression is finally obtained:

$$U(\boldsymbol{R}_1, \boldsymbol{p}) = \int d\boldsymbol{R}_2 \frac{1}{(\sqrt{\pi}\mu)^3} e^{-\frac{1}{\mu^2}(\boldsymbol{R}_1 - \boldsymbol{R}_2)^2} U_{NM}(\boldsymbol{p}; k_F(R_2)). \tag{30}$$

This is the form of the improved LDA by a Gaussian form factor $\frac{1}{(\sqrt{\pi}\mu)^3} e^{-\frac{1}{\mu^2}(\boldsymbol{R}_1 - \boldsymbol{R}_2)^2}$. The range μ introduced in Eq. (26) corresponds to the range β in Eq, (8).

The major assumption in the above derivation is the factorization given in Eq. (26). The plausibility of this replacement for the real part is the following. The first observation is that the contribution of the second term with the factor of $(-1)^{S+T}$ is originated from the antisymmetrization and works to retain the allowed spin, isospin, and partial-wave channels. That is, the direct and exchange contributions are same. Second, the momentum $\boldsymbol{x}$ in the direct part is momentum transfer, and the momentum-transfer dependence can be described by a local potential. Supposing that the dominant contribution to the nuclear mean field is represented by a single Gaussian with a range of μ in the coordinate space, $e^{-(r/\mu)^2}$, as a function of the distance r, the expression of Eq. (26) holds. For example, the two-range Gaussian Gogny force [17] that has been widely used for nuclear mean-field calculations has the range $\mu = 1.2$ fm in the main attractive part. The range μ in Eq, (26) is expected to be close to this value. Actually, the range used in the improved LDA calculations in Sec. II A is $\beta \approx 1.0$ fm. On the other hand, the above reasoning may not be easily applied to the imaginary part, and consequently the improved LDA is less reliable as is demonstrated in Sec. II B.

It is noted that only the single-particle central potential is obtained in nuclear matter. The single-particle spin-orbit potential, which is essentially important in the properties of nuclei, is left out in the present calculation.

IV. SUMMARY

To derive OMPs in finite nuclei based on the two-body G matrices in nuclear matter, a G-matrix folding method has been commonly employed. In this method, G matrices in nuclear matter are parametrized as energy- and density-dependent effective interactions in a convenient local-function form and they are applied to construct an OMP in a finite nucleus by a folding procedure. There is another calculationally less demanding LDA method, in which a single-particle potential in nuclear matter is directly related to the potential in a finite nucleus at the position corresponding to the nuclear matter density. To compensate for the lack of finite-range effects, a Gaussian folding is introduced, which is called an improved LDA. The latter method does not require substantial efforts to parametrize G matrices. Although the improved LDA with an appropriate Gaussian range has been practically successful, it is worthwhile to add theoretical studies of the properties of the method. To assess the usability of the improved LDA, numerical and analytical studies are carried out.

In the first part, explicit numerical calculations in the two methods are presented for ^{40}Ca, ^{90}Zr, and ^{208}Pb at the energies $E = 65$ and 100 MeV, starting from the same G matrices [9] in nuclear matter with chiral nucleon-nucleon and three-nucleon interactions [23,24]. The improved LDA potentials are shown to have a good correspondence to the G-matrix folding potentials in the real part. These microscopic OMPs also correspond well to the phenomenological potentials parametrized by Koning and Delaroche [16], when a Pauli rearrangement potential, the second-order Pauli-blocking effect, is taken into account [10], which is not included in the lowest-order microscopic calculation. The imaginary part, however, does not show a good resemblance between the two methods, even if the finite-range correction is applied. It is also observed that the G-matrix folding imaginary potential differs from the Koning and Delaroche empirical potential, especially in the central region. Nevertheless, the calculated nucleon elastic cross sections with microscopic OMPs are similar to those of the Koning and Delaroche potential at $E = 65$ MeV, as is shown in Sec. II C. Because observables of nucleon-nucleus scattering are almost determined by the OMP of the surface area when the nucleon incident energy is not large, the description of the elastic scattering in insensitive to the potential strength in the central region. The overestimation of the imaginary strength of the OMP in a nuclear matter approach is common in the literature [8,11,18]. The microscopic understanding of the imaginary OMP needs further investigations.

In Sec. III, the relation between the improved LDA method and the G-matrix folding method is examined analytically, introducing reasonable assumptions of the Slater approximation of the density-matrix expansion and the localization by the Wigner transformation. It is shown that if the approximation of Eq. (26) is accepted, the Gaussian folding expression of the improved LDA is recovered. This approximation is reasonable for the real part, but probably not credible for the imaginary part. Keeping these features in mind, it is useful to apply the improved LDA method in other situations such as hyperons [25].

ACKNOWLEDGMENTS

The author is indebted to M. Toyokawa for evaluating the OMPs in the G-matrix folding method. This work is supported by JSPS KAKENHI Grant No. JP16K17698.

[1] K. A. Brueckner, J. L. Gammel, and H. Weitzner, Phys. Rev. **110**, 431 (1958).
[2] J. P. Jeukenne, A. Lejeune, and C. Mahaux, Phys. Rev. C **10**, 1391 (1974).
[3] J. P. Jeukenne, A. Lejeune, and C. Mahaux, Phys. Rep. **25**, 83 (1976).
[4] J. P. Jeukenne, A. Lejeune, and C. Mahaux, Phys. Rev. C **16**, 80 (1977).
[5] F. A. Brieva and J. R. Rook, Nucl. Phys. A **291**, 299 (1977).
[6] F. A. Brieva and J. R. Rook, Nucl. Phys. A **291**, 317 (1977).
[7] K. Amos, P. J. Dortmans, H. V. von Geramb, S. Karataglidis, and J. Raynal, in *Advances in Nuclear Physics*, edited by J. W. Negele and E. Vogt (Plenum, New York, 2000), Vol. 25, p. 275.
[8] T. Furumoto, Y. Sakuragi, and Y. Yamamoto, Phys. Rev. C **78**, 044610 (2008).
[9] M. Toyokawa, M. Yahiro, T. Matsumoto, and M. Kohno, Prog. Theor. Exp. Phys. **2018**, 023D03 (2018).
[10] M. Kohno, Phys. Rev. C **98**, 054617 (2018).
[11] T. R. Whitehead, Y. Lim, and J. W. Holt, Phys. Rev. C **100**, 014601 (2019).
[12] K. Minomo, K. Ogata, M. Kohno, Y. R. Shimizu, and M. Yahiro, J. Phys. G **37**, 085011 (2010).
[13] J. C. Slater, Phys. Rev. **81**, 385 (1951).
[14] J. W. Negele and D. Vautherin, Phys. Rev. C **5**, 1472 (1972).
[15] M. Kohno, Phys. Rev. C **88**, 064005 (2013); **96**, 059903(E) (2017).
[16] A. J. Koning and J. P. Delaroche, Nucl. Phys. A **713**, 231 (2003).
[17] J. F. Berger, M. Girod, and D. Gogny, Comput. Phys. Commun. **63**, 365 (1991).
[18] N. Yamaguchi, S. Nagata, and T. Matsuda, Prog. Theor. Phys. **70**, 459 (1983).
[19] M. Toyokawa, M. Yahiro, T. Matsumoto, K. Minomo, K. Ogata, and M. Kohno, Phys. Rev. C **92**, 024618 (2015); **96**, 059905(E) (2017).
[20] H. Sakaguchi, M. Nakamura, K. Hatanaka, A. Goto, T. Noro, F. Ohtani, H. Sakamoto, H. Ogawa, and S. Kobayashi, Phys. Rev. C **26**, 944 (1982).
[21] H. Sakaguchi, M. Nakamura, K. Hatanaka, A. Goto, T. Noro, F. Ohtani, H. Sakamoto, and S. Kobayashi, Phys. Lett. B **89**, 40 (1979).
[22] H. Horiuchi, Prog. Theor. Phys. **64**, 184 (1980).
[23] E. Epelbaum, W. Göckle, and U.-G. Meißner, Nucl. Phys. A **747**, 362 (2005).
[24] E. Epelbaum, A. Nogga, W. Glöckle, H. Kamada, Ulf-G. Meißner, and H. Witala, Phys. Rev. C **66**, 064001 (2002).
[25] M. Kohno, Phys. Rev. C **100**, 024313 (2019).